Harnessing host enhancers of SARS-CoV-2 entry as novel targets for antiviral therapy

Williams, Nathalia; Silva, Filo; Schmolke, Mirco

How to cite

WILLIAMS, Nathalia, SILVA, Filo, SCHMOLKE, Mirco. Harnessing host enhancers of SARS-CoV-2 entry as novel targets for antiviral therapy. In: Antiviral research, 2024, vol. 228, p. 105951. doi: 10.1016/j.antiviral.2024.105951

This publication URL: https://archive-ouverte.unige.ch/unige:178648
Publication DOI: 10.1016/j.antiviral.2024.105951

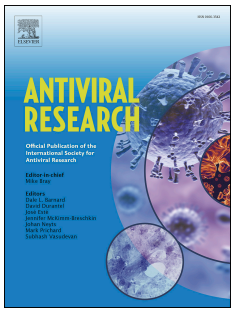

Harnessing host enhancers of SARS-CoV-2 entry as novel targets for antiviral therapy

Nathalia Williams, Filo Silva, Mirco Schmolke

PII: S0166-3542(24)00160-8

DOI: https://doi.org/10.1016/j.antiviral.2024.105951

Reference: AVR 105951

To appear in: *Antiviral Research*

Received Date: 26 January 2024

Revised Date: 18 June 2024

Accepted Date: 26 June 2024

Please cite this article as: Williams, N., Silva, F., Schmolke, M., Harnessing host enhancers of SARS-CoV-2 entry as novel targets for antiviral therapy, *Antiviral Research*, https://doi.org/10.1016/j.antiviral.2024.105951.

Harnessing host enhancers of SARS-CoV-2 entry as novel targets for antiviral therapy

Nathalia Williams[1], Filo Silva[1], Mirco Schmolke[1,2]*

[1] Department of Microbiology and Molecular Medicine, Faculty of Medicine, University of Geneva, Geneva, Switzerland

[2] Geneva Center for inflammation research, Faculty of Medicine, University of Geneva, Geneva, Switzerland

*contact: mirco.schmolke@unige.ch

Key words: SARS-CoV-2, Coronavirus, Covid-19, virus entry, receptor, antiviral

Short title: Novel host targets for antiviral therapy against SARS-CoV-2

Abstract

The WHO declared the official end of the SARS-CoV-2 caused public health emergency on May 5th, 2023, after two years in which the virus infected approximately 750 Mio individuals causing estimated up to 7 Mio deaths. Likely, the virus will continue to evolve in the human population as a seasonal respiratory pathogen. To now prevent severe infection outcomes in vulnerable individuals, effective antivirals are urgently needed to complement the protection provided by vaccines. SARS-CoV-2 enters its host cell via ACE2 mediated membrane fusion, either at the plasma membrane, if the protease TMPRSS2 is present or via the endosome, in a cathepsin dependent fashion. A small number of positive regulators of viral uptake were described in the literature, which are potentially useful targets for host directed antiviral therapy or biomarkers indicating increased or diminished susceptibility to infection. We identified here by cell surface proximity ligation novel proteins, required for efficient virion uptake. Importantly, chemical inhibition of one of these factors, SLC3A2, resulted in robust reduction of viral replication, to that achieved with a TMPRSS2 inhibitor. Our screen identified new host dependency factors for SARS-CoV-2 entry, which could be targeted by novel antiviral therapies.

Introduction

At the end of 2019 a novel SARS Coronavirus (SARS-CoV-2) entered the human population[1], presumably after a zoonotic transfer from a yet to be identified animal source. The virus quickly spread globally, infected more than 750 Mio people and is responsible for at almost 7 million deaths (WHO, https://covid19.who.int, Dec 2023). SARS-CoV-2 replicates in the upper

and occasionally lower respiratory tract of humans. Infections can remain asymptomatic; symptomatic infections manifest in a wide range: from cold-like symptoms to acute respiratory distress syndrome and respiratory failure[2].

SARS-CoV-2 virions attach to heparan sulfates on the cell surface and rely primarily on angiotensin converting enzyme 2 (ACE2) to enter the host cell[3]. The entry process requires proteolytic activation of the SARS-CoV-2 spike[4] (S) and either occurs at the cell surface, when the serin protease TMPRSS2 is expressed by the host cell or by endosomal uptake[3]. In the latter case endosomal cathepsins are responsible for the cleavage of SARS-CoV-2 S protein, initiating fusion of viral and endosomal membrane[5].

In vivo, expression of hACE2 suffices to make mice susceptible to SARS-CoV-2. Additional entry factors such as neuropilin 1 were identified, which support ACE2 dependent entry [6]. However, ACE2 independent entry was shown, e.g., in H522 cells. Here ACE2 knockout did not affect the entry process, suggesting that additional proteins could substitute the default receptor[7]. Along these lines, S protein mutations found in variants of concern, which lead to enhanced viral entry, do not augment ACE2 binding[8]. This points to additional host dependency factors permitting or supporting the entry process of SARS-CoV-2.

To identify such host factors, we here used cell surface proximity ligation (CSPL[9]) to identify host plasma membrane proteins in the vicinity of attached viral spike proteins. Hits were validated with subsequent gain of function and loss of function approaches using VLP entry assays. Using chemical inhibitors of a subset of entry factors in virus infection assays we ultimately demonstrate that these host surface proteins could serve as future drug targets in antiviral therapy.

Results

We previously applied cell surface proximitiy ligation (CSPL) to biotin-label host plasma membrane protein in the vicinity of attached trimeric viral ligands[9]. Coupled to mass spectrometry this strategy successfully identified TfR1 as a host entry factor for influenza A viruses[9]. Here, we performed CSPL on A549 cells overexpressing ACE2 and TMPRSS2 (A549 A2T2 (Fig.S1A and B)). As molecular bait we used a stabilized trimeric SARS-CoV-2 S protein[10] and fused it C-terminally to HRP. These proteins were produced in insect cell culture using a baculovirus expression system (Fig. S1C). When incubating A549 A2T2 cells with this bait and applying its substrate biotin phenol we achieved biotin ligation to numerous host proteins, which were pulled down with streptavidin beads and analysed by mass spectrometry (Fig.1A). Data from three independent CSPL/MS experiments were filtered against the cell surface proteome atlas[11] and cross-referenced with the CRAPome library[12] for contaminants frequently found in pulldown-MS experiments. As comparator we used pulldown data from cells incubated with trimeric HRP only. We also considered hits that were found in at least two out of three experiments (n=55) (Fig.1B and Table S1). Among these were known host entry factors of SARS-CoV-2, such as neuropilin 1 (NRP1)[6]. The *bona fide* host entry receptor for SARS-CoV-2, ACE2, was only found enriched in one out of three experiments. Encouragingly, from the short list of 55 proteins about half were grouped into the GO cluster *viral entry into host cells* (GO:0046718, red), *virus life cycle* (GO: 0019058, green) and *virus receptor activity* (GO:0001618, blue) Fig 1C) with false discovery rates of 7.08×10^{-19}, 1.02×10^{-17} and 5.32×10^{-18}, respectively. In contrast proteins that did not fulfill our bioinformatics selection criteria grouped into virus receptor activity (GO:0001618) with an FDR of 0.0067, the other two biological processes were not associated with this group of proteins (Fig. S2). We continued

with a hand-picked selection of ten candidates indicated by a black circle in Fig 1C (five assigned to GO:0046718 and or GO:0001618, and five without such assignment). We next depleted all ten proteins with at least two gRNAs using CRISPR/Cas9 and subsequent single cell cloning in A549 A2T2 cells. Successful knockouts were confirmed by western blot (WB) and whenever possible we continued with two clones, one from each gRNA approach (Fig. S3, selected clones are marked with an asterisk). As positive control we used ACE2 knockout A549 cells (based on A549 A2T2). To assess the functional consequences of genetic depletion of surface proteins on SARS-CoV-2 entry we infected knockout and control cells with SARS-CoV-2 S pseudotyped replication incompetent HIV based VLP encoding a Gaussia luciferase reporter[13]. To assess specificity, we used in parallel VSV G pseudotyped VLP. Since the two VLP differ only in the surface protein, distinct effects of knockout are most probably related to early steps of viral replication (attachment, entry, fusion). The infectious dose was harmonized between SARS-CoV-2 S and VSV G pseudotyped VLP, as measured by the absolute luciferase activity. We also made sure that both VLP dilutions resulted in comparable absolute light units in the luciferase assay (Fig.S4). Genetic depletion of five out of ten proteins resulted in robust reduction of SARS-CoV-2 S pseudotyped VLP entry (Fig. 2A and Z-score in 2C). Amongst these, knockout of three target genes (ATP1B1, ADAM10 and SLC3A2) resulted in comparable loss of infection as knockout of ACE2 (Fig. 2A), suggesting an important effect on VLP entry. In contrast, none of the ten clones had a significant effect on the entry of VSV G pseudotyped VLP (Fig. 2B and and Z-score in 2D). Of note, we excluded those of the 10 candidates (Table S1) for which knockout results (Fig. S3) and entry assay (Fig. S5) gave inconsistent results (e.g. when two gRNA resulted in robust knockout but only one in a functional reduction of entry).

To assess the function of the remaining five proteins in a less artificial overexpression cell system, we turned to Calu3 cells, which express both ACE2 and the serine protease

TMPRSS2[14]. Since these cells divide poorly in cell culture, we applied a bulk knockout approach using lentiviral expressed CRISPR/Cas9 followed by puromycin selection. Knockout efficacy was confirmed by WB. Only those cell populations with at least 50% reduction in protein levels in the bulk population were used for functional assays (Fig. S6, A) WB and B) quantification). Of note, the endogenous levels of the six candidates differed between A549 A2T2 and Calu3 cells (Fig. S6C), notably ADAM10 and ATP1B1 were substantially lower in A549 A2T2, while SLC3A2 levels were slightly higher. Knockout of all candidates except ATP1B1 resulted in significantly reduced entry of SARS-CoV-2 S pseudotyped VLP in Calu3 cells (Fig. 3), while VSV G pseudotyped VLP entry was not significantly affected. Notably, the knockout of EGFR, which only reduced the entry into A549 A2T2 cells by about 50% (with a rather weak Z score) had a much stronger effect in Calu3 cells, potentially in consequence of the generally lower levels of endogenously expressed ACE2 (Fig. S1B), which could make entry less efficient in Calu3 cells. Overall, we found a large overlap of candidate knockouts that significantly affected SARS-CoV-2 VLP entry in the two different cell lines. It should however be noted that the extent, to which each of these knockouts affects VLP entry differed between the two cell lines. This could be a consequence of the higher or lower ACE2 and TMPRSS2 density (Fig. S1). We next asked whether increasing the endogenous levels of the identified entry factor candidates in host cells would positively affect VLP entry. Since A549 A2T2 are already highly infectable, we decided to use parental A549 cells and A549 cells solely overexpressing ACE2 (A549 A2) (Fig. S1B). Additionally, we overexpressed the candidate cDNAs in Calu3 cells. However, in contrast to the clear affects achieved by knockout approaches, overexpression of the respective cDNAs by lentiviral transduction into either A549, A549-ACE2 or Calu3 cells did not enhance VLP infection, potentially due to sufficient endogenous amounts of entry factors (Fig. S7-9). Overexpression of entry factors was confirmed by specific WB (Fig. S10).

Some viruses downregulate their own entry receptors in infected host cells to avoid reinfection of the same cell during the exit process[15-17]. We reasoned that a downregulation of proviral entry factors could prevent SARS-CoV-2 reinfection of the same cell. Protein levels for the factors described here were analyzed by WB 24 h post infection. Both entry factors that supported SARS-CoV-2 S pseudotyped VLP entry in Calu3 cells, EGFR, ADAM10 and SLC3A2, were downregulated during SARS-CoV-2 infection. Importantly, this downregulation was specific since alternative host surface proteins (PLXNB2 and ATP1B1) remained unaffected by virus infection (Fig. 4).

While multiple vaccine platforms were successfully implemented and saved millions of lives in the Covid-19 pandemic, successful antiviral therapy options are still limited. ADAM10 was recently identified as an alternative protease cleaving SARS-CoV-2 S[18]. For the here identified most potent host entry factors ADAM10, ATP1B1 and SLC3A2 (identified in A549 A2T2) small molecule inhibitors are commercially available (Table S2)[19,20,45,47]. The TMPRSS2 inhibitor Camostat was included as a positive control. Using a Cell titer glo viability assay we determined the highest non-toxic concentration when applying it on Calu3 cells (Fig. S11 A-D). Cells were pretreated for 2 h with 100 µM of Camostat, 100 µM or 500 µM of KYT0353 (LAT1-SLC3A2 inhibitor also known as JPH203) or 100 µM of ouabain (ATP1B1 inhibitor) and 4 h with 100 µM of GI254023X (ADAM10 inhibitor). The incubation time for the chemical compounds was determined using published data[19,20,45,47]. After the incubation with the chemical compounds, cells were washed and infected with MOI 1 of SARS-CoV-2 Omicron BA.1. Viral RNA copies of subgenomic E RNA were determined by qRT-PCR 24 h post infection (Fig.5A-C). Treatment with KYT0353 at both 100 µM and 500 µM reduced the viral charge robustly (Fig.5A and B), performing comparably to the TMPRSS2 inhibitor Camostat (Fig.5C). Of note, while the the

166 higher concentration of KYT0353 reduced viral replication below the limit of detection at 24h
167 we also observed a reduction cell viability to 80% (Fig. S11B), suggesting a certain degree of
168 toxicity. In contrast chemical inhibition of ADAM10 or ATP1B1 had little or no effect,
169 respectively (Fig.5A and C).
170 In summary our data show that CSPL-identified host surface proteins can serve as novel
171 antiviral drug targets for the inhibition of SARS-CoV-2 entry.

Discussion

Over the past three years, several host factors have been described, which enhance SARS-CoV-2 entry. Amongst these are ADAM10 and ADAM17[18], MMP2 and MMP9[21] and TMPRSS13[22]. None of these replaces ACE2 as main receptor for virion entry[23]. Instead, these host factors promote cleavage of SARS-CoV-2 S (ADAM17) or act through a yet unknown but ACE2 dependent entry mechanism. TMEM106B in contrast was recently shown to allow ACE2 independent entry into cells[24], suggesting that SARS-CoV-2 is more flexible in its entry mechanism than initially thought.

We here describe the identification of five host entry factors of SARS-CoV-2: ATP1B1, SLC3A2, ADAM10, PLXNB2 and EGFR using an unbiased approach via cell surface proximity ligation. Our data hence confirm independently the role of ADAM10 in virus entry[18].

Importantly three of the remaining four factors were already implicated in the entry of other human viruses. SLC3A2 was described to support entry of another positive strand RNA virus, HCV[25], without affecting other steps of virus replication. ATP1B1 interacts with influenza A and B virus M2 protein, which is essential for acidification of the virion during entry. Knockout of the ATP1B1 gene in MDCK cells reduced replication of influenza A viruses, suggesting this host factor is required for virus entry[26]. It was further proposed to act positively on cell to cell spread of HCMV[27] by an unknown mechanism. Conversely, ATP1B1 induction was shown to upregulate innate antiviral responses via TRAF3 and TRAF6[28].

EGFR was proposed as a proviral entry factor or entry receptor of a number of human viruses: influenza A viruses[29,30], HBV[31], HCV[32], HEV[33], HPV[34], ZiV[35] or TGEV[36]. Only for plexin B2 we did not find a known direct implication in the entry process or the replication of other viruses. It should be pointed out, that in our hands plexin B2 did not play a significant role in entry of SARS-CoV-2 into Calu3 cells.

196

197 This suggests that diverse viruses evolved convergent entry strategies relying of overlapping
198 host surface proteins to overcome the host plasma membrane. In consequence some of these
199 proteins might be excellent targets for broad-spectrum antiviral therapies.
200 We previously used CSPL to identify host proteins involved in influenza A virus entry[9]. Our data
201 here show that this technique could have broader implications for other viruses to identify
202 host entry factors or potentially host restriction factors of entry. We also noticed that CSPL
203 was substantially more reproducible using SARS-CoV-2 S as compared to the previously used
204 influenza virus HA. Potentially this is a consequence of a more selective protein receptor use
205 by SARS-CoV-2 to enter cells, while IAV tends to show rather promiscuous receptor use[37].
206 Consequently, we speculate that the protein environment at the point of entry is more defined
207 for SARS-CoV-2 than for IAV.
208 Curiously we found that SARS-CoV-2 infection diminishes the levels of some proviral entry
209 factors found here, e.g. SLC3A2 and ADAM10, while increasing the levels of the *bona fide* entry
210 receptor ACE2. In contrast plexin B2 levels remained stable during infection. This might
211 suggest that the virus selectively targets a certain group of cell surface proteins. The
212 mechanisms leading to these reduced protein levels need to be addressed in future studies,
213 but they could be linked to virus induced shutoff by nsp1. We postulate that this reduction of
214 host surface proteins enhancing viral entry, would be beneficial for the virus when exiting
215 infected cells to avoid reinfection.
216 Our data might also contribute to the ongoing search for host factors contributing to enhanced
217 or reduced susceptibility of human patients[38,39]. Expression levels and sequence variations in
218 the here identified entry supporting factors might explain why some patients are more
219 sensitive to SARS-CoV-2 infection.

Direct antivirals against SARS-CoV-2 approved for clinical use include ritonavir-boosted nirmatrelvir (Paxlovid), remdesivir and molnupiravir. Host directed therapies aim mostly at a dampened inflammatory response to limit immune pathology[40]. Currently there are no antiviral strategies approved that target host dependency factors, but few are in clinical trials[41,42].

Knockout of SLC3A2 resulted in comparable reduction of VLP entry as ACE2 knockout. Importantly chemical targeting of SLC3A2 diminished replication of recent SARS-CoV-2 strain to similar extent as that of the TMPRSS2 inhibitor Camostat. In complex with LAT1 SLC3A2 forms a well characterized heterodimeric transporter at the plasma membrane for large neutral amino acids[43]. It remains to be elucidated if the inhibition of SARS-CoV-2 entry via chemical blocking of SLC3A2 relies on the presence of LAT1 or occurs in an independent fashion.

Concluding, our data suggest that targeting of SLC3A2 might provide a new avenue of host directed antiviral therapy against SARS-CoV-2, either alone or in combination with other antivirals. These therapies are urgently needed to complement the successful vaccine approaches in place.

Limitations of our study: The compounds used in Fig. 5 are not approved antivirals. The aim of our study was to demonstrate that a surface proximity ligation approach can be used to identify druggable surface proteins for novel antiviral therapies. At the same time a lack of antiviral effect of some of these compounds does not exclude that other inhibitors or blocking antibodies against the identified HDF could be exploited for antiviral therapy. We can further not rule out that the untested 45 surface proteins identified by CSPL contain additional HDF with druggable potential. Future studies will have to clarify this point.

Materials and Methods

Cell lines

HEK293T (human embryonic kidney, ATCC) were cultured in DMEM (Dulbecco's modified eagle medium, Gibco 10566016) A549 (adenocarcinomic human alveolar basal epithelial cells, ATCC), A549 A2 and A459 A2T2 cell lines and all derived cell lines including the knockout and over expression cell lines, were grown in DMEM/F12 + GlutaMAX (Dulbecco's Modified Eagle Medium/Nutrient Mixture F-12, Gibco #10565018). For the A549 and A549 A2 over expression cell lines, the culture medium was supplemented with 2 µg/ml of puromycin and 6 µg/ml of blasticidin. Calu3 (lung epithelial adenocarcinoma cells, ATCC) and Calu3 derived knockout and over expression cell lines were grown in MEM + GlutaMAX (Gibco #41090-28) + 1x MEM non-essential amino acids 100X (Gibco #11140-035) + 10 mM HEPES (Gibco #15630-056) + 1mM sodium pyruvate (Gibco #11360-039). Cell culture media were supplemented with 10 % (v/v) heat-inactivated foetal bovine serum (Gibco #10270-106. Lot: 2307592) and pen-strep antibiotics (100 U/ml penicillin and 0.1 mg/ml streptomycin, Sigma-Aldrich #P0781). For Calu3 knockout and over expression cell lines, the growth medium was supplemented with either puromycin at 4ug/ml or with blasticidin at 2 µg/ml. All cells were maintained in low passage at 37 °C with 5 % CO2 and 90 % humidity, absence of mycoplasma was routinely confirmed by PCR.

SDS- PAGE and Western Blot

For western blot analysis, the cells were lysed in protein lysis buffer (tris Hcl 1 M pH 6.8, glycerol, SDS 20 %, H2O and DTT), sonicated 10X (30 secs on and 30 secs off) at 4°C and boiled at 95°C for 5 min . The samples were separated on a 7% SDS-PAGE gel and the transfer was

performed to nitrocellulose filter membranes 0.45µM at 120V for 2 h. The membranes were blocked by 5 % skim milk, blotted with primary antibodies followed by incubation with horseradish peroxidase HRP conjugated secondary antibodies and visualised using enhanced chemiluminescent reagent (#K12049-D50) from Advansta.

Plasmids

pLVX-IRES-Puro was purchased from Clontech (#632183). pSpCas9(BB)-2A-GFP (PX458) was a gift from Feng Zhang (Addgene #48138) and pMD2.G and psPAX2 were a gift from Didier Trono (Addgene #12259 and #12260).

Oligonucleotides for gRNA cloning and PCR primers

All oligonucleotides were purchased from Microsynth (France). Guide RNAs were designed using CRISPick and cloned into LentiCRISPR v2 (Addgene #52961) for Calu3 cells and into pSpCas9 (BB)-2A-GFP for A549 A2T2 cells (Addgene #48138). Two gRNAs were chosen to target each gene hence the nomenclature gRNA1 and gRNA2.

Guide RNA (gRNA)	Sequences 5'-3'
ACE2_gRNA1_fwd	CACCGTCCTGTGCAGATATTACACA
ACE2_gRNA1_rev	AAACTGTGTAATATCTGCACAGGAC
ACE2_gRNA2_fwd	CACCGCAGGATCCTTATGTGCACAA
ACE2_gRNA2_rev	AAACTTGTGCACATAAGGATCCTGC
ALCAM_gRNA1_fwd	CACCGTGTGTGCATGCTAGTAACTG
ALCAM_gRNA1_rev	AAACCAGTTACTAGCATGCACACAC
ALCAM_gRNA2_fwd	CACCGCTTACACACTGACGGATGTG

ALCAM_gRNA2_rev	AAACCACATCCGTCAGTGTGTAAGC
ATP1B1_gRNA1_fwd	CACCGGGAGACTTTAATCATGAACG
ATP1B1_gRNA1_rev	AAACCGTTCATGATTAAAGTCTCCC
ATP1B1_gRNA2_fwd	CACCGTCCAAGGACTCATTCTTGGG
ATP1B1_gRNA2_rev	AAACCCCAAGAATGAGTCCTTGGAC
CD44_gRNA1_fwd	CACCGCTTGATGACCTCGTCCCATG
CD44_gRNA1_rev	AAACCATGGGACGAGGTCATCAAGC
CD44_gRNA2_fwd	CACCGGCAATATGTGTCATACTGGG
CD44_gRNA2_rev	AAACCCCAGTATGACACATATTGCC
EGFR_gRNA1_fwd	CACCGTGTCACCACATAATTACCTG
EGFR_gRNA1_rev	AAACCAGGTAATTATGTGGTGACAC
EGFR_gRNA2_fwd	CACCGTCTTGCCGGAATGTCAGCCG
EGFR_gRNA2_rev	AAACCGGCTGACATTCCGGCAAGAC
EPHA2_gRNA1_fwd	CACCGCAAGTTGCCAGATCCCTCCG
EPHA2_gRNA1_rev	AAACCGGAGGGATCTGGCAACTTGC
EPHA2_gRNA2_fwd	CACCGCGAGGTCACTTACCGCAAGA
EPHA2_gRNA2_rev	AAACTCTTGCGGTAAGTGACCTCGC
ITGAV_gRNA1_fwd	CACCGGGAATTGATAGCGTATCTGC
ITGAV_gRNA1_rev	AAACGCAGATACGCTATCAATTCCC
ITGAV_gRNA2_fwd	CACCGAGGCAATAGAGATTATGCCA
ITGAV_gRNA2_rev	AAACTGGCATAATCTCTATTGCCTC
ITGB4_gRNA1_fwd	CACCGCTGCGAGATCAACTACTCGG
ITGB4_gRNA1_rev	AAACCCGAGTAGTTGATCTCGCAGC
ITGB4_gRNA2_fwd	CACCGCTACTCCTATAGCTACTACG
ITGB4_gRNA2_rev	AAACCGTAGTAGCTATAGGAGTAGC

SLC3A2_gRNA1_fwd	CACCGCAGGCCCGTGAACTTAGCCG
SLC3A2_gRNA1_rev	AAACCGGCTAAGTTCACGGGCCTGC
SLC3A2_gRNA2_fwd	CACCGGCGCAGAAGTGGTGGCACAC
SLC3A2_gRNA2_rev	AAACGTGTGCCACCACTTCTGCGCC
ADAM10_gRNA1_fwd	CACCGCCCATAAATACGGTCCTCAG
ADAM10_gRNA1_rev	AAACCTGAGGACCGTATTTATGGGC
ADAM10_gRNA2_fwd	CACCGGAAGGATTCATCCAGACTCG
ADAM10_gRNA2_rev	AAACCGAGTCTGGATGAATCCTTCC
PLXNB2_gRNA1_fwd	CACCGTTCCACGGCGATATCCAGTG
PLXNB2_gRNA1_rev	AAACCACTGGATATCGCCGTGGAAC
PLXNB2_gRNA2_fwd	CACCGCACCTGGCAAAGCTTCGTAG
PLXNB2_gRNA2_rev	AAACCTACGAAGCTTTGCCAGGTGC
NECTIN2_gRNA1_fwd	CACCGGCGAGTTCAAGTGCTACCCG
NECTIN2_gRNA1_rev	AAACCGGGTAGCACTTGAACTCGCC
NECTIN2_gRNA2_fwd	CACCGACACTCACAGCGTACAGAGA
NECTIN2_gRNA2_rev	AAACTCTCTGTACGCTGTGAGTGTC

284

285

286 PCR primers used for cloning to make over expression plasmids are indicated below.

Primer	**Sequence 5'-3'**
EPHA2_fwd	GGCGCTCGAGACCATGGAGCTCCAGGCAGC
EPHA2_rev	GGCGTCTAGACTAGATGGGGATCCCCACA
NECTIN2_fwd	GCGGGAATTCATGGCCCGGGC
NECTIN2_rev	GCGGGGATCCTCACACATACATGGCC
ITGAV_fwd	GCGGGAATTCACCATGGCTTTTCCGCCGCGGC

ITGAV_rev	GCGGGGATCCTTAAGTTTCTGAGTTT
ADAM10_fwd	GCGGACCTCGAGATGGTGTTGCTGAG
ADAM10_rev	GCGGGCGGCCGCTTA

Antibodies

Mouse monoclonal against actin antibody (#ab49900), rabbit monoclonal against Adam10 antibody (#ab124695, epr5622) and rabbit monoclonal against ACE2 antibody (#ab272500, epr24705-45) were purchased from Abcam. Mouse monoclonal anti-FLAG HRP antibody (#A8592), goat polyclonal anti-rabbit IgG HRP antibody (#A8275) and goat polyclonal anti-mouse IgG HRP antibody (#A5278) were purchased from Sigma-Aldrich. The streptavidin-HRP (#S-911) was purchased from Thermofisher. Rabbit polyclonal against ITGB4 (#21738-1-AP), mouse monoclonal against ALCAM (#67768-1-Ig), rabbit polyclonal against PLXNB2 (#10602-1-AP), rabbit polyclonal against SLC3A2 (#15193-1-A), mouse monoclonal EGFR (#66455-1-Ig), mouse monoclonal EPHA2 (#66736-1-Ig), rabbit polyclonal ITGAV (#27096-1-AP) and rabbit polyclonal anti-goat IgG HRP antibody (#SA00001-4) were purchased from Proteintech. Rabbit polyclonal anti-ATP1B1 antibody (#HAP012911) was purchased from Atlas antibodies. Goat polyclonal against NECTIN2 antibody (#AF2229) was purchased from R&D Systems. Mouse monoclonal against CD44 antibody (#156-3C11) was purchased from Cell Signaling Technology.

Inhibitors

TMPRSS2 specific inhibitor Camostat mesylate (#SML0057) were purchased from Sigma-Aldrich. Ouabain (#1076) an ATPase inhibitor, KYT0353 (#5026) an inhibitor of LAT1/SLC3A2

were purchased from Tocris. GI254023X targeting ADAM10 (#SML0789) were purchased from Sigma-Aldrich.

Recombinant proteins

Trimeric Spike was previously described[10]. Based on this sequence (GenBank accession no. MN908947.3 for the original sequence), we added the coding sequence for HRP on the 3' end of the T4foldon, connected via a GSGSG-linker and followed by a His10-tag. A trimerized HRP control was designed with the same T4foldon and His10 tag. The recombinant proteins were expressed and purified at the Protein core facility (CMU, University of Geneva) using the baculovirus (Sf9 insect cells) expression system. Baculovirus were generated using a modified pFastBac vector encoding C-terminally tagged i) Wuhan Spike, ii) no protein. The proteins had a C-terminal tag composed of fused Wuhan Spike - HRP and a 10-histidine tag. The media containing the proteins was centrifuged at 4000 x g for 15 min at 4°C and filtered using 0.22 µm filters. The media was concentrated and adjusted to 10mM imidazole and applied on to a 5 ml His-trap FF column (Cytiva). 100ml of PBS supplemented with 1M NaCl and 10mM Imidazole was used to wash the column and the column was eluted with 15ml of elution buffer (1 x PBS, 200 mM NaCl, 450 mM imidazole). Proteins eluted were concentrated to 1ml using AMICON 30 MWCO concentrators and loaded on a Size Exclusion Chromatography Superdex 200 10/300 column equilibrated in PBS at 4 °C. Pure protein fractions were pooled, concentrated and flash frozen in liquid nitrogen.

Cell surface proximity ligation assay

A549, A549 A2, A549 A2T2 and Calu3 cells were grown in 6-well format and incubated with 100 µg of recombinant Spike-HRP or HRP alone for 60 min. Biotin phenol and H_2O_2 were added

for 10 min to allow proximity ligation of biotin. Cells were quenched and lysed with lysis buffer (0.4 % SDS, 500mM NaCl, 5 mM EDTA, 50 mM Tris-HCl pH 7.5, 1 % Triton-X100, 1 mM DTT, protease inhibitor). Biotinylated proteins were precipitated with streptavidin-agarose beads (Thermofisher #11205D) and prepared for mass spectrometry by on bead trypsin digest.

Mass spectrometry

On bead trypsin digestion was done to digest the proteins and peptides were analysed by nanoLC-MSMS using an easynLC1000 (Thermo Fisher) coupled to a Qexactive Plus mass spectrometer (Thermo Fisher). Data were analysed with Scaffold (Proteome Software) with 1 % of protein FDR with a 0.1 % of peptide FDR. Cell surface protein atlas was used to cross reference the proteins. For identification of host surface proteins enriched in the proximity of the Wuhan spike-HRP, the following cutoffs were applied: 1) 2-fold enrichment of Wuhan spike HRP over control HRP, 2) atleast 2 unique peptide per protein, 3) proteins present in less than 200 experiments out of 716 streptavidin dependent pulldowns in the CRAPome database.

Generation of a KO cell line using CRISPR/Cas9 with lentiviral transduction for Calu3

Subconfluent HEK293T cells in 6-well plates were transfected at a ratio of 1:3:4 with the following plasmids pMD2.G (vesicular stomatitis virus G protein (VSV G)), psPAX2 (HIV gag-pol) were a gift from Didier Trono (Addgene plasmid # 12259 and #12260) and lentiCRISPRv2, a gift from Feng Zhang (Addgene plasmid # 52961)[44] containing the specific gRNA (see above) with 2 µg/µl of Trans-lT LT1 (Mirus). After 24 h, HEK293T medium was replaced with target cell medium. Calu3 cells were seeded in 6-well plates at a density of 50 %. The HEK293T supernatants containing lentiviruses to knockout the target protein was harvested 48h post transfection with a syringe and was passed through a sterile filter of 0.45µM and

356 complemented with polybrene at 8 µg/ml. The supernatant-polybrene mix was added to
357 Calu3 cells after washing the cells 1X with PBS. The supernatant containing lentiviruses were
358 removed from Calu3 cells after 4 h and replaced with respective growth medium. At 48 h post
359 transduction, Calu3 cells were split and selected with puromycin at 4 µg/ml. The knockout
360 efficiency was assessed using western blot.
361
362 **Generation of a KO cell line using CRISPR/Cas9 for A549 A2T2**
363 Subconfluent levels of A549 A2T2 in 6-well plates were transfected with 2 µg of the target
364 protein knockout plasmids (vector backbone pSpCas9(BB)-2A-GFP from Addgene #48138)[45]
365 using FuGENE HD transfection reagent (Promega #E2311). 4 h post transfection, the medium
366 was removed from A549 A2T2 cells and replaced with growth medium. 48 h post transfection,
367 green fluorescent protein (GFP)-positive cells were sorted using Beckman Coulter MoFlo
368 Astrios individually into 96-well plates. The efficiency of knockout was verified by western
369 blotting. The cell lines transfected with an empty plasmid pSpCas9(BB)-2A-GFP are indicated
370 as Cas9 empty.
371
372 **Generation of overexpressing cell lines with lentiviral transduction systems**
373 HEK293T cells in 6-well plates, at sub confluency, were transfected at a ratio of 1:3:4 with the
374 following plasmids pMD2.G (vesicular stomatitis virus G protein (VSV G)), psPAX2 (HIV gag-
375 pol) and over expression plasmids using 2 µl/µg of Trans-lT LT1 (Mirus). 24 h post transfection,
376 293T medium was replaced with target cell medium. Target cells (A549, A549 A2 and Calu3)
377 were seeded in 6-well plates. The HEK293T supernatants containing lentiviruses were
378 harvested 48h post transfection with a syringe and were passed through a 0.45 µm sterile
379 filter. These lentiviruses were complemented with 8 µg/ml of polybrene. Target cells were

washed 1X with PBS following transduction with 2 ml of lentivirus-polybrene mix. 4 h after transduction, lentiviruses were removed from target cells and replaced with respective growth medium. 48 h post transduction, target cells were split and selected using puromycin at 2 µg/ml for A549 and A549 A2, 4 µg/ml for Calu3 and blasticidin at 6 µg/ml for A549 and A549 A2 and 2 µg/ml for Calu3. The efficiency of over expression was verified by western blot.

SARS-CoV-2 Virus-Like Particles (VLP) production

To generate replication incompetent, luciferase expressing VLP, subconfluent 100 mm dish 293T cells were transfected with: 10 µg of psPAX, 5 µg of pCG1 SARS-CoV-2 Spike[46] or 2.5 µg of pMD2.G and 15 µg of CD510B Gluc (vector backbone pCDH-CMV-MCS-EF1-Puro from Sanbio, Netherlands #CD510B-1) kindly provided by Fabien Abdul, University of Geneva, using Trans lT-LT1 transfection reagent (Mirus) according to manufacturer's instructions. The supernatant containing SARS-CoV-2 Spike and VSV G pseudotyped VLP were harvested 48 h and 72 h post transfection, respectively. The supernatants were cleared from cell debris by centrifugation (2000 x g, 10 min, 4°C) and were passed through a 0.45 µm filter attached to a syringe to remove cell debris. Aliquots were stored at -80 °C. VLP stocks were titered on target cells to achieve comparable infection rates within the linear range of the luciferase assay.

Titration of SARS-CoV-2 and VSV G VLPs on Cas9 empty and ACE2KO cells

Subconfluent Calu3 Cas9 empty, Calu3 ACE2KO and Calu3 ACE2*KO in 96-well plates were transduced with different volumes of the both SARS-CoV-2 and VSV G VLPs. 6 h post transfection, the VLPs were removed from the cells, washed 2X with 300ul of PBS per well and replaced with appropriate growth medium. The supernatant was collected every 24 h until 96 h, washed 2X with PBS and replaced with growth medium. After the harvest, the supernatants

were centrifuged at 1500 x g for 7 min. 5 µl of the supernatant was then mixed with 50 µl of coelenterazine (Biosynth #EC175526) on white plates and the luciferase activity was measured using the Dual Glo protocol on the Glomax 96-well microplate luminometer.

Infection with SARS-CoV-2 VLP

Calu3, A549, A549 A2 and A549 A2T2 were seeded to achieve subconfluency in 96-well plates pre-coated with poly-L-lysine. The cells were washed once with PBS and infected with 100 µl of SARS-CoV-2 Spike or VSV G pseudotyped VLP per well. 6 h post-infection, the VLP were removed, the cells were washed twice with PBS and 100 µl of fresh medium (MEM + GlutaMAX (Gibco #41090-28) + 1x MEM non-essential amino acids 100X (Gibco #11140-035) + 10mM HEPES (Gibco #315630-056) + 1mM sodium pyruvate (Gibco #11360-039) + 10 % (v/v) heat-inactivated foetal bovine serum (Gibco #10270-106. Lot: 2307592) + pen-strep antibiotics (100 U/ml penicillin and 0.1 mg/ml streptomycin, Sigma-Aldrich #P0781)) was added to each well. 96 h post-infection, the supernatants were collected and subjected to centrifugation. The Gaussia luciferase activity was measured by adding 5 µL of the supernatant with 50 µL of coelenterazine (Biosynth #EC175526) on white plates using the Glomax 96-well microplate luminometer Promega. DualGlo protocol in the Glomax software was used for the measurement which was at a rate of 1 s per well.

SARS-CoV-2 virus production

Calu3 cells were grown in 100 mm dish at sub-confluency. The cells were infected with an MOI of 0.01 of Omicron and pre-VOC B.1 (kindly provided by Prof. Isabella Eckerle) viruses for 1 h at 37 °C in MEM + GlutaMAX (Gibco #41090-28) + 1x MEM non-essential amino acids 100X (Gibco #11140-035) + 10mM HEPES (Gibco #15630-056) + 1 mM sodium pyruvate (Gibco

#311360-039) + pen-strep antibiotics (100 U/ml penicillin and 0.1 mg/ml streptomycin, Sigma-Aldrich #P0781) + 2% (v/v) heat-inactivated fetal bovine serum (Gibco #10270-106. Lot: 2307592). The inoculum was removed after 1 h and fresh medium was added. The viral supernatants were recovered 48 h and 96 h post-infection for Omicron and Wuhan, respectively. The supernatants were centrifuged at 450 x g for 5 min and stored at -70 °C.

Plaque assay to determine viral titers.

Vero E6 TMPRSS2 cells were grown to form a monolayer in 24-well plates. The cells were infected with 200 µl of serially diluted viruses. Viruses were diluted in serum free DMEM medium (Gibco #10566016). 1 h post infection, the inoculum was removed and 2.4 % Avicel overlay (Dupont) was added to the cells. Cells were incubated for 96h for both viruses at 37 °C. The overlay was removed, then cells were fixed in 4 % formaldehyde and the cell monolayer was stained with a solution of crystal violet. Plaques were counted and multiplied with the dilution and volume factor to determine viral titers (pfu/ml).

Cell Titer Glo cell viability assay

Calu3 cells were seeded in 96-well plates, at sub confluent levels, the cells were washed 1X with PBS and the different chemical inhibitors Camostat mesylate (100 µM), GI254023X (100 µM), Ouabain (10 nM) and KYT0353 (100 µM and 500 µM) were added to the cells in medium with 2 % fetal bovine serum (FBS). The cells were pre-incubated with Camostat mesylate, Ouabain and KYT0353 individually for 2 h and with GI254023X for 4 h according to published data[19,20,45,47]. The chemical compounds were removed every (2 h or 4 h) + 24 h for 4 days. Cells were washed and lysed by agitation using cell titer glo reagent at 450 rpm for 5 min using an orbital shaker. After 10 min incubation of the plate at room temperature, 180

µl of the mix was transferred to a luminometer-compatible, 96-well white plate. The luminescence signal was recorded on GloMax luminometer with preset Cell titer Glo protocol.

SARS-CoV-2 infection after pre-treatment with chemical inhibitors

Calu3 cells at subconfluency in 24-well plates were pre-incubated with different chemical compounds. 2 h incubation was performed for Camostat mesylate (100 µM), Ouabain (10 nM) and KYT0353 (100 or 500µM) and 4 h incubation was performed for GI254023X (100 µM) according to published data[19,20,45,47]. At the end of the incubation time, the chemical inhibitors were removed and cells were washed 1X with PBS and were infected with Omicron (BA.1: EPI_ISL_7605546) SARS-CoV-2 virus at a MOI of 1. After 45 min of incubation with the virus, the inoculum was removed, the cells were washed 1X with PBS and was replaced by respective growth medium with 2 % FBS + 1 % P/S. For the higher concentration of KYT0353 (500 µM), after removal of virus inoculum, cells were washed with PBS and replaced by respective growth medium with 2 % FBS + 1 % P/S containing 500 µM of KYT0353. 24 h post infection, the cells were washed 1X with PBS and lysed in TRK lysis buffer (OmegaBiotek #R6834) for RT qPCR analysis. Samples were inactivated for 10 min at 70°C and exported from the BSL3 laboratory.

SARS-CoV-2 infection in Calu3 cells to determine expression of target proteins.

Calu3 cells were seeded in 12 well plates to achieve subconfluency. They were infected with pre-Voc (B.1: EPI_ISL_414019) and Omicron (BA.1: EPI_ISL_7605546) SARS-CoV-2 virus at a MOI of 1. After 45 mins of incubation with the virus, the inoculum was removed, the cells were washed 1X with PBS. The wells were replaced by respective growth medium with 2 %

FBS + 1 % P/S. 24 h post infection, cells were washed and lysed with protein lysis buffer (tris Hcl 1 M pH 6.8, glycerol, SDS 20 %, H2O and DTT), sonicated 10X (30 secs on and 30 secs off) at 4°C and boiled at 95°C for 5 min for western blot analysis.

Reverse Transcription quantitative PCR

For extraction of total RNA from cells, EZNA total RNA kit I (OmegaBiotek #R6834) was used according to manufacturers' instructions. Either probe based or SYBR green based assays were used to detect the different RNAs. The probe-based assay was used to detect subgenomic E (sgE) and RNaseP. For quantitative RT-PCR, a 25 µl reaction with 5ul of RNA was done with the Superscript III 1-step reverse transcriptase-PCR system (Invitrogen) with the Platinum Taq DNA polymerase according to the manufacturers' protocol. Probes contained a 5' YY-520 reporter dye and MGB 3' quencher for subgenomic E (sgE) and 5' FAM-520 reporter dye and MGB 3' quencher for RNase P (Hs04930436, #4331182), both purchased from Microsynth. To determine the early virus replication, a quantitative RT-PCR targeting the subgenomic RNA encoding the envelope (sgE) was performed. The RT-PCR was performed using a thermocycling protocol with reverse transcription for 15 min at 50 °C and a denaturation step for 2 min at 95 °C to restore Taq DNA polymerase activity, followed by PCR amplification by 45 cycles of 95 °C for 15 s and 60 °C for 30 s. Fluorescence signal was detected after the elongation step of each cycle. RT-PCR was done with the following primers and probe: nCoV sgE Fwd: 5'-CCAACCAACTTTCGATCTCTTGT-3', nCoV sgE Rev: 5'- CGTACCTGTCTCTTCCGAAACG-3' and nCoV sgE prb: 5'YY/ TCTCTAAACGAACTTATGTACTC/ 3'MGB – Q530. 18S and GAPDH were detected using SYBR green system. RT was performed with 100ng of RNA samples for all conditions. The qPCR was performed using 1ul of cDNA mixed with 10ul of 2X KAPA SYBR FAST qPCR Master Mix-universal (KAPA Biosystems, USA). 0.5ul of each of the forward and reverse

primers (10µM) were added to the mix to make a final volume of 20ul with RNase, DNase water. qPCR was performed following a thermocycling protocol of an initial denaturation step at 95 °C for 5 min, followed by 40 cycles of denaturation at 95 °C for 30 s and annealing/extension at 60 °C for 60 s. The following primers were used 18S Fwd: GTAACCCGTTGAACCCCATT, 18S Rev: CCATCCAATCGGTAGTAGCG, GAPDH Fwd: GCAAATTTCCATGGCACCGT and GAPDH Rev: GCCCCACTTGATTTTGGAGG. The normalized change in relative subgenomic E (sgE) gene expression was calculated by delta-delta CT method and by using average expression of 3 housekeeping genes, RNaseP, 18S and GAPDH.

Statistics

Statistical analysis was performed using GraphPad Prism 9. Statistical tests applied are indicated in each respective figure legend.

Funding sources

This work was funded by the SNSF31CA30_196330 granted to MS.

Acknowledgements

We are thankful for the professional support from the following core facilities: Protein core facility, Proteomics, FACS, BSL3 at the CMU. We thank the group of Prof. Isabella Eckerle for providing us with the SARS-CoV-2 isolates and the group of KH Krause, especially Fabien Abdul for the HIV-VLP system and A549 A2T2 cells.

References

1 Zhu, N. *et al.* A Novel Coronavirus from Patients with Pneumonia in China, 2019. *N Engl J Med* **382**, 727-733 (2020). https://doi.org:10.1056/NEJMoa2001017

2 Chen, G. *et al.* Clinical and immunological features of severe and moderate coronavirus disease 2019. *J Clin Invest* **130**, 2620-2629 (2020). https://doi.org:10.1172/JCI137244

3 Hoffmann, M. *et al.* SARS-CoV-2 Cell Entry Depends on ACE2 and TMPRSS2 and Is Blocked by a Clinically Proven Protease Inhibitor. *Cell* **181**, 271-280 e278 (2020). https://doi.org:10.1016/j.cell.2020.02.052

4 Jackson, C. B., Farzan, M., Chen, B. & Choe, H. Mechanisms of SARS-CoV-2 entry into cells. *Nat Rev Mol Cell Biol* **23**, 3-20 (2022). https://doi.org:10.1038/s41580-021-00418-x

5 Ou, X. *et al.* Author Correction: Characterization of spike glycoprotein of SARS-CoV-2 on virus entry and its immune cross-reactivity with SARS-CoV. *Nat Commun* **12**, 2144 (2021). https://doi.org:10.1038/s41467-021-22614-1

6 Daly, J. L. *et al.* Neuropilin-1 is a host factor for SARS-CoV-2 infection. *Science* **370**, 861-865 (2020). https://doi.org:10.1126/science.abd3072

7 Puray-Chavez, M. *et al.* Systematic analysis of SARS-CoV-2 infection of an ACE2-negative human airway cell. *Cell Rep* **36**, 109364 (2021). https://doi.org:10.1016/j.celrep.2021.109364

8 Hoffmann, M. *et al.* Evidence for an ACE2-Independent Entry Pathway That Can Protect from Neutralization by an Antibody Used for COVID-19 Therapy. *mBio* **13**, e0036422 (2022). https://doi.org:10.1128/mbio.00364-22

9 Mazel-Sanchez, B. *et al.* Influenza A virus exploits transferrin receptor recycling to enter host cells. *Proc Natl Acad Sci U S A* **120**, e2214936120 (2023). https://doi.org:10.1073/pnas.2214936120

10 Weiss, S. *et al.* A High-Throughput Assay for Circulating Antibodies Directed Against the S Protein of Severe Acute Respiratory Syndrome Coronavirus 2. *J Infect Dis* **222**, 1629-1634 (2020). https://doi.org:10.1093/infdis/jiaa531

11 Bausch-Fluck, D. *et al.* A mass spectrometric-derived cell surface protein atlas. *PLoS One* **10**, e0121314 (2015). https://doi.org:10.1371/journal.pone.0121314

12 Mellacheruvu, D. *et al.* The CRAPome: a contaminant repository for affinity purification-mass spectrometry data. *Nat Methods* **10**, 730-736 (2013). https://doi.org:10.1038/nmeth.2557

13 Ilmjarv, S. *et al.* Concurrent mutations in RNA-dependent RNA polymerase and spike protein emerged as the epidemiologically most successful SARS-CoV-2 variant. *Sci Rep* **11**, 13705 (2021). https://doi.org:10.1038/s41598-021-91662-w

14 Hoffmann, M. *et al.* Chloroquine does not inhibit infection of human lung cells with SARS-CoV-2. *Nature* **585**, 588-590 (2020). https://doi.org:10.1038/s41586-020-2575-3

15 Tanaka, M. *et al.* Downregulation of CD4 is required for maintenance of viral infectivity of HIV-1. *Virology* **311**, 316-325 (2003). https://doi.org:10.1016/s0042-6822(03)00126-0

16 Welstead, G. G., Hsu, E. C., Iorio, C., Bolotin, S. & Richardson, C. D. Mechanism of CD150 (SLAM) down regulation from the host cell surface by measles virus hemagglutinin protein. *J Virol* **78**, 9666-9674 (2004). https://doi.org:10.1128/JVI.78.18.9666-9674.2004

17 Lindwasser, O. W., Chaudhuri, R. & Bonifacino, J. S. Mechanisms of CD4 downregulation by the Nef and Vpu proteins of primate immunodeficiency viruses. *Curr Mol Med* **7**, 171-184 (2007). https://doi.org:10.2174/156652407780059177

18 Jocher, G. *et al.* ADAM10 and ADAM17 promote SARS-CoV-2 cell entry and spike protein-mediated lung cell fusion. *EMBO Rep* **23**, e54305 (2022). https://doi.org:10.15252/embr.202154305

19 Seifert, A. *et al.* The metalloproteinase ADAM10 requires its activity to sustain surface expression. *Cell Mol Life Sci* **78**, 715-732 (2021). https://doi.org:10.1007/s00018-020-03507-w

20 Oda, K. *et al.* L-type amino acid transporter 1 inhibitors inhibit tumor cell growth. *Cancer Sci* **101**, 173-179 (2010). https://doi.org:10.1111/j.1349-7006.2009.01386.x

21 Benlarbi, M. *et al.* Identification and differential usage of a host metalloproteinase entry pathway by SARS-CoV-2 Delta and Omicron. *iScience* **25**, 105316 (2022). https://doi.org:10.1016/j.isci.2022.105316

22 Stevaert, A. *et al.* Impact of SARS-CoV-2 Spike Mutations on Its Activation by TMPRSS2 and the Alternative TMPRSS13 Protease. *mBio* **13**, e0137622 (2022). https://doi.org:10.1128/mbio.01376-22

23 Bestle, D. *et al.* TMPRSS2 and furin are both essential for proteolytic activation of SARS-CoV-2 in human airway cells. *Life Sci Alliance* **3** (2020). https://doi.org:10.26508/lsa.202000786

24 Baggen, J. *et al.* TMEM106B is a receptor mediating ACE2-independent SARS-CoV-2 cell entry. *Cell* **186**, 3427-3442 e3422 (2023). https://doi.org:10.1016/j.cell.2023.06.005

25 Nguyen, N. N. T. *et al.* Hepatitis C Virus Modulates Solute carrier family 3 member 2 for Viral Propagation. *Sci Rep* **8**, 15486 (2018). https://doi.org:10.1038/s41598-018-33861-6

26 Mi, S., Li, Y., Yan, J. & Gao, G. F. Na(+)/K (+)-ATPase beta1 subunit interacts with M2 proteins of influenza A and B viruses and affects the virus replication. *Sci China Life Sci* **53**, 1098-1105 (2010). https://doi.org:10.1007/s11427-010-4048-7

27 Cui, X. *et al.* Interaction between human cytomegalovirus UL136 protein and ATP1B1 protein. *Braz J Med Biol Res* **44**, 1251-1255 (2011). https://doi.org:10.1590/s0100-879x2011007500144

28 Cao, W. *et al.* Inducible ATP1B1 Upregulates Antiviral Innate Immune Responses by the Ubiquitination of TRAF3 and TRAF6. *J Immunol* **206**, 2668-2681 (2021). https://doi.org:10.4049/jimmunol.2001262

29 Eierhoff, T., Hrincius, E. R., Rescher, U., Ludwig, S. & Ehrhardt, C. The epidermal growth factor receptor (EGFR) promotes uptake of influenza A viruses (IAV) into host cells. *PLoS Pathog* **6**, e1001099 (2010). https://doi.org:10.1371/journal.ppat.1001099

30 Sieben, C., Sezgin, E., Eggeling, C. & Manley, S. Influenza A viruses use multivalent sialic acid clusters for cell binding and receptor activation. *PLoS Pathog* **16**, e1008656 (2020). https://doi.org:10.1371/journal.ppat.1008656

31 Iwamoto, M. *et al.* Epidermal growth factor receptor is a host-entry cofactor triggering hepatitis B virus internalization. *Proc Natl Acad Sci U S A* **116**, 8487-8492 (2019). https://doi.org:10.1073/pnas.1811064116

32 Lupberger, J. *et al.* EGFR and EphA2 are host factors for hepatitis C virus entry and possible targets for antiviral therapy. *Nat Med* **17**, 589-595 (2011). https://doi.org:10.1038/nm.2341

33 Schrader, J. A. *et al.* EGF receptor modulates HEV entry in human hepatocytes. *Hepatology* **77**, 2104-2117 (2023). https://doi.org:10.1097/HEP.0000000000000308

34 Bannach, C. *et al.* Epidermal Growth Factor Receptor and Abl2 Kinase Regulate Distinct Steps of Human Papillomavirus 16 Endocytosis. *J Virol* **94** (2020). https://doi.org:10.1128/JVI.02143-19

35 Sabino, C., Bender, D., Herrlein, M. L. & Hildt, E. The Epidermal Growth Factor Receptor Is a Relevant Host Factor in the Early Stages of The Zika Virus Life Cycle In Vitro. *J Virol* **95**, e0119521 (2021). https://doi.org:10.1128/JVI.01195-21

36 Hu, W., Zhang, S., Shen, Y. & Yang, Q. Epidermal growth factor receptor is a co-factor for transmissible gastroenteritis virus entry. *Virology* **521**, 33-43 (2018). https://doi.org:10.1016/j.virol.2018.05.009

37 Sempere Borau, M. & Stertz, S. Entry of influenza A virus into host cells - recent progress and remaining challenges. *Curr Opin Virol* **48**, 23-29 (2021). https://doi.org:10.1016/j.coviro.2021.03.001

38 Bastard, P. *et al.* Autoantibodies against type I IFNs in patients with life-threatening COVID-19. *Science* **370** (2020). https://doi.org:10.1126/science.abd4585

39 Zhang, Q., Bastard, P., Effort, C. H. G., Cobat, A. & Casanova, J. L. Human genetic and immunological determinants of critical COVID-19 pneumonia. *Nature* **603**, 587-598 (2022). https://doi.org:10.1038/s41586-022-04447-0

40 Qin, Z. *et al.* Effect of anti-inflammatory drugs on the storm of inflammatory factors in respiratory tract infection caused by SARS-CoV-2: an updated meta-analysis. *Front Public Health* **11**, 1198987 (2023). https://doi.org:10.3389/fpubh.2023.1198987

41 Reuschl, A. K. *et al.* Host-directed therapies against early-lineage SARS-CoV-2 retain efficacy against B.1.1.7 variant. *bioRxiv* (2021). https://doi.org:10.1101/2021.01.24.427991

42 Varona, J. F. *et al.* Preclinical and randomized phase I studies of plitidepsin in adults hospitalized with COVID-19. *Life Sci Alliance* **5** (2022). https://doi.org:10.26508/lsa.202101200

43 Kahlhofer, J. & Teis, D. The human LAT1-4F2 hc (SLC7A5-SLC3A2) transporter complex: Physiological and pathophysiological implications. *Basic Clin Pharmacol Toxicol* **133**, 459-472 (2023). https://doi.org:10.1111/bcpt.13821

44 Sanjana, N. E., Shalem, O. & Zhang, F. Improved vectors and genome-wide libraries for CRISPR screening. *Nat Methods* **11**, 783-784 (2014). https://doi.org:10.1038/nmeth.3047

45 Ran, F. A. *et al.* Genome engineering using the CRISPR-Cas9 system. *Nat Protoc* **8**, 2281-2308 (2013). https://doi.org:10.1038/nprot.2013.143

46 Hoffmann, M., Kleine-Weber, H. & Pohlmann, S. A Multibasic Cleavage Site in the Spike Protein of SARS-CoV-2 Is Essential for Infection of Human Lung Cells. *Mol Cell* **78**, 779-784 e775 (2020). https://doi.org:10.1016/j.molcel.2020.04.022

45 Ko, M.; Chang, S.Y.; Byun, S.Y.; Ianevski, A.; Choi, I.; Pham Hung d'Alexandry d'Orengiani, A.-L.; Ravlo, E.; Wang, W.; Bjørås, M.; Kainov, D.E.; et al. Screening of FDA-Approved Drugs Using a MERS-CoV Clinical Isolate from South Korea Identifies Potential Therapeutic Options for COVID-19. *Viruses* **2021**, *13*, 651. https://doi.org/10.3390/v13040651

46 Gheware, A., Ray, A., Rana, D. *et al.* ACE2 protein expression in lung tissues of severe COVID-19 infection. *Sci Rep* **12**, 4058 (2022). https://doi.org/10.1038/s41598-022-07918-6

47 Madoux, F., Dreymuller, D., Pettiloud, JP. *et al.* Discovery of an enzyme and substrate selective inhibitor of ADAM10 using an exosite-binding glycosylated substrate. *Sci Rep* **6**, 11 (2016). https://doi.org/10.1038/s41598-016-0013-4

48 Carriquí-Madroñal B, Sheldon J, Duven M, Stegmann C, Cirksena K, Wyler E, Zapatero-Belinchón FJ, Vondran FWR, Gerold G. The matrix metalloproteinase ADAM10 supports hepatitis C virus entry and cell-to-cell spread via its sheddase activity. PLoS Pathog. 2023 Nov 15;19(11):e1011759. doi: 10.1371/journal.ppat.1011759. PMID: 37967063; PMCID: PMC10650992.

49 Schmidt K, Keller M, Bader BL, Korytář T, Finke S, Ziegler U, Groschup MH. Integrins modulate the infection efficiency of West Nile virus into cells. J Gen Virol. 2013 Aug;94(Pt 8):1723-1733. doi: 10.1099/vir.0.052613-0. Epub 2013 May 8. PMID: 23658209; PMCID: PMC3749529.

50 Lyle C, McCormick F. Integrin alphavbeta5 is a primary receptor for adenovirus in CAR-negative cells. Virol J. 2010 Jul 8;7:148. doi: 10.1186/1743-422X-7-148. PMID: 20615244; PMCID: PMC2909962.

51 Garrigues HJ, Rubinchikova YE, Dipersio CM, Rose TM. Integrin alphaVbeta3 Binds to the RGD motif of glycoprotein B of Kaposi's sarcoma-associated herpesvirus and functions as an RGD-dependent entry receptor. J Virol. 2008 Feb;82(3):1570-80. doi: 10.1128/JVI.01673-07. Epub 2007 Nov 28. PMID: 18045938; PMCID: PMC2224453.

52 Gianni T, Salvioli S, Chesnokova LS, Hutt-Fletcher LM, Campadelli-Fiume G. αvβ6- and αvβ8-integrins serve as interchangeable receptors for HSV gH/gL to promote endocytosis and activation of membrane fusion. PLoS Pathog. 2013;9(12):e1003806. doi: 10.1371/journal.ppat.1003806. Epub 2013 Dec 19. PMID: 24367260; PMCID: PMC3868510.

53 Ngan, Ngo & Lim, Yun-Sook & Nguyen, Lap P. & Tran, Cong Si & Luong, Trang & Nguyen, Tram & Pham, Hang & Mai, Han & Choi, Jae-Woong & Han, Sang-Seop & Hwang, Bum-Soon. (2018). Hepatitis C Virus Modulates Solute carrier family 3 member 2 for Viral Propagation. Scientific Reports. 8. 10.1038/s41598-018-33861-6.

54 Lupberger J, Zeisel MB, Xiao F, Thumann C, Fofana I, Zona L, Davis C, Mee CJ, Turek M, Gorke S, Royer C, Fischer B, Zahid MN, Lavillette D, Fresquet J, Cosset FL, Rothenberg SM, Pietschmann T, Patel AH, Pessaux P, Doffoël M, Raffelsberger W, Poch O, McKeating JA, Brino L, Baumert TF. EGFR and EphA2 are host factors for hepatitis C virus entry and possible targets for antiviral therapy. Nat Med. 2011 May;17(5):589-95. doi: 10.1038/nm.2341. Epub 2011 Apr 24. PMID: 21516087; PMCID: PMC3938446.

55 Noh SS, Shin HJ. Role of Virus-Induced EGFR Trafficking in Proviral Functions. *Biomolecules*. 2023; 13(12):1766. https://doi.org/10.3390/biom13121766

56 Chen J, Sathiyamoorthy K, Zhang X, Schaller S, Perez White BE, Jardetzky TS, Longnecker R. Ephrin receptor A2 is a functional entry receptor for Epstein-Barr virus. Nat Microbiol. 2018 Feb;3(2):172-180. doi: 10.1038/s41564-017-0081-7. Epub 2018 Jan 1. PMID: 29292384; PMCID: PMC5972547.

57 Martinez WM, Spear PG. Structural features of nectin-2 (HveB) required for herpes simplex virus entry. J Virol. 2001 Nov;75(22):11185-95. doi: 10.1128/JVI.75.22.11185-11195.2001. PMID: 11602758; PMCID: PMC114698.

58 Warner MS, Geraghty RJ, Martinez WM, Montgomery RI, Whitbeck JC, Xu R, Eisenberg RJ, Cohen GH, Spear PG. A cell surface protein with herpesvirus entry activity (HveB) confers susceptibility to infection by mutants of herpes simplex virus type 1, herpes

simplex virus type 2, and pseudorabies virus. Virology. 1998 Jun 20;246(1):179-89. doi: 10.1006/viro.1998.9218. PMID: 9657005.

59 Ogawa H, Fujikura D, Namba H, Yamashita N, Honda T, Yamada M. Nectin-2 Acts as a Viral Entry Mediated Molecule That Binds to Human Herpesvirus 6B Glycoprotein B. Viruses. 2022 Jan 16;14(1):160. doi: 10.3390/v14010160. PMID: 35062364; PMCID: PMC8779676.

60 Evander M, Frazer IH, Payne E, Qi YM, Hengst K, McMillan NA. Identification of the alpha6 integrin as a candidate receptor for papillomaviruses. J Virol. 1997 Mar;71(3):2449-56. doi: 10.1128/JVI.71.3.2449-2456.1997. PMID: 9032382; PMCID: PMC191355.

61 Evander M, Frazer IH, Payne E, Qi YM, Hengst K, McMillan NA. Identification of Fothergill T, McMillan NA. Papillomavirus virus-like particles activate the PI3-kinase pathway via alpha-6 beta-4 integrin upon binding. Virology. 2006 Sep 1;352(2):319-28. doi: 10.1016/j.virol.2006.05.002. Epub 2006 Jun 15. PMID: 16781758.

62 Recalde-Reyes DP, Rodríguez-Salazar CA, Castaño-Osorio JC, Giraldo MI. PD1 CD44 antiviral peptide as an inhibitor of the protein-protein interaction in dengue virus invasion. Peptides. 2022 Jul;153:170797. doi: 10.1016/j.peptides.2022.170797. Epub 2022 Apr 1. PMID: 35378215; PMCID: PMC10807690.

Figure legends

Figure 1: Cell surface proximity ligation. A) Pulldown of biotinylated host cell proteins on A549 A2T2 cells with streptavidin post cell surface proximity ligation. Streptavidin-HRP was used to probe biotinylated proteins**. B)** Venn diagram indicating number of proteins found in the three mass spectrometry experiments and their overlap in A549 A2T2 cells. 6 proteins that overlapped between the 3 experiments are: ADAM10, CD109, CD44, ITGA3, ITGA6 and ITGAV. **C)** Half of the hits found in two out of three experiments were grouped into the GO cluster for viral entry into host cells and virus receptor activity. Black circle indicates the hand-picked candidates.

Figure 2: SARS-CoV-2 S and VSV-G pseudotyped VLP entry into A549 A2T2 KO cells. A) SARS-CoV-2 pseudotyped VLP entry in A549 A2T2 cells transduced with lentiviral CRISPR/Cas9 guide RNAs (2 per target). ACE2 is used as a positive control. The results are shown in relative light units to mock, Cas9 empty. The results of the 2 guide RNAs are pooled together. One-way ANOVA with Brown-Forsythe and Welch test was done. **B)** VSV-G pseudotyped VLP entry in A549 A2T2 cells transduced with lentiviral CRISPR/Cas9 guide RNAs (2 per target). ACE2 is used as a positive control. The results are shown in relative light units to mock, Cas9 empty. The results of the 2 guide RNAs are pooled together. One-way ANOVA with Brown-Forsythe and Welch test was done. **C)** Z-score analysis depicting the effect of the knockout of 5 out of 10 candidates on SARS-CoV-2 S pseudotyped VLP entry. The dotted lines at -3 and +3 are thresholds that correspond to 3 times the standard deviation. **D)** Z-score showing the effect of the knockout of 5 out of 10 protein candidates on VSV-G pseudotyped VLP entry. The dotted lines at -3 and +3 are thresholds that correspond to 3 times the standard deviation.

Figure 3: SARS-CoV-2 S and VSV-G pseudotyped VLP entry into Calu3 KO cells. A) SARS-CoV-2 pseudotyped VLP entry in Calu3 cells transduced with lentiviral CRISPR/Cas9 guide RNAs (2 per target). ACE2 is used as a positive control. The results are shown in relative light units to mock, Cas9 empty. The results of the 2 guide RNAs are pooled together. One-way ANOVA with Brown-Forsythe and Welch test was done. **B)** VSV-G pseudotyped VLP entry in Calu3 cells transduced with lentiviral CRISPR/Cas9 guide RNAs (2 per target). ACE2 is used as a positive control. The results are shown in relative light units to mock, Cas9 empty. The results of the 2 guide RNAs are pooled together. One-way ANOVA with Brown-Forsythe and Welch test was done. **C)** Z-score analysis depicting the effect of the knockout of the proteins on SARS-CoV-2 S pseudotyped VLP entry. The dotted lines at -3 and +3 are thresholds that correspond to 3 times the standard deviation. **D)** Z-score showing the effect of the knockout of the proteins on VSV-G pseudotyped VLP entry. Dotted lines at -3 and +3 are thresholds that correspond to 3 times the standard deviation.

Figure 4: SARS-CoV-2 regulates the expression of some of the target proteins. A) Cell lysates were separated by SDS-PAGE and analyzed by western blot depicting the expression of target proteins and SARS-CoV-2 N, 24 h post infection with pre-VOC B.1 and Omicron BA.1 at MOI 1. A representative blot of three independent experiments is shown. Equal loading was confirmed by probing for beta actin. **B-G)** Quantification of three independent infection experiments as shown in (A) for ACE2, ATP1B1, SLC3A2, ADAM10, EGFR, PLNXB2 across B to G, respectively. Statistical significance was determined with a one-way ANOVA test.

Figure 5: SARS-CoV-2 replication post-treatment with chemical inhibitors of ADAM10, SLC3A2, TMPRSS2 and ATP1B1 A) Treatment of Calu3 cells with KYT0353 (100 µM) for 2h or

778 GI254023X (100µM) for 4 h. Post incubation with inhibitor, cells were washed and infected
779 with MOI 1 of Omicron BA.1. RT-qPCR was performed after RNA extraction from cell lysates
780 collected 24 h post infection to assess for subgenomic E gene. Each dot represents a biological
781 replicate indicated as relative expression to the average of the housekeeping genes, RNaseP,
782 18S and GAPDH. Ordinary one-way ANOVA was performed as a statistical test. **B)** Treatment
783 of Calu3 cells with KYT0353 at a concentration of 500 µM for 2 h. The cells were washed to
784 remove the compound and infected with Omicron BA.1 at a MOI of 1. After removal of the
785 virus inoculum, cells were washed and replaced with growth medium containing KYT0353
786 (500 µM). RT-qPCR was done to assess subgenomic E gene from cell lysates 2 h + 24 h post
787 incubation. Each dot represents a biological replicate shown as relative expression to the
788 average of RNaseP, 18S and GAPDH. A paired T-test was performed to analyze the statistical
789 significance between the Mock and chemical inhibition. **C)** Treatment of Calu3 cells with
790 Camostat mesylate (100 µM) and Ouabain (10 nM) for 2 h. Post incubation, the chemical
791 compounds were removed, cells were washed and infected with MOI 1 of Omicron BA.1. RT-
792 qPCR was performed after RNA extraction from cell lysates collected 2 h + 24 h post incubation
793 to assess for subgenomic E gene. Each dot represents a biological replicate indicated as
794 relative expression to the average of the housekeeping genes, RNaseP, 18S and GAPDH.
795 Ordinary one-way ANOVA was performed as a statistical test.
796
797 **Figure S1: A)** Summary of CSPL technique generated with BioRender.com. B) Cell lysates with
798 40ug of proteins were separated by SDS-PAGE and analysed by western blot depicting the
799 expression of ACE2 in different cell lines (A549, A549 A2, A549T2, A549 A2T2, H522 and Calu3
800 WT). Both short and long exposures have been shown to visualize the ACE2 bands in the
801 different cell lines. Beta-actin was used as a loading control. **C)** Representative SDS-PAGE of

802 insect cell expresses Wuhan-spike HRP. Purified protein containing fractions were loaded onto
803 an SDS-polyacrylamide gel and stained with Coomassie Blue.
804
805 **Figure S2:** String network of the 55 proteins found in mass spectrometry in the three
806 independent experiments in A549 A2T2 cells, according to gene ontology classification and
807 sorted from lowest to highest false discovery rate (FDR).
808
809 **Figure S3:** Total cell lysates were separated by SDS-PAGE and analyzed by western blot to
810 confirm knockouts of target proteins in A549 A2T2 cells. ACE2 knockout in A549 A2T2 cells
811 was done as a positive control. Equal loading was verified by probing for beta-actin. The
812 asterisk refers to the single-cell knockout clones that were used for the experiments for each
813 gRNA and for each target.
814
815 **Figure S4:** Absolute luciferase values after infection of Calu3 control (Cas9 empty) or ACE2 KO
816 cells 96h post infection. VLPs were psudotyped with SARS-CoV-2 S (**A**) or VSV-G (**B**) and diluted
817 to achieve a comparable absolute infection efficacy. Each dot represents a technical replicate
818 in one biological experiment.
819
820 **Figure S5: A)** SARS-CoV-2 S pseudotyped VLP entry in A549 A2T2 knockout cells (Fig S3). The
821 asterisk represents the knockout of the target proteins using a 2nd gRNA. The results are shown
822 in relative light units to mock, Cas9 empty. One-way ANOVA with Brown-Forsythe and Welch
823 test was done. **B)** VSV-G VLP entry in A549 A2T2 cells knockout for the candidates. The asterisk
824 indicates knockout using a 2nd gRNA. The results are shown in relative light units to mock, Cas9
825 empty. One-way ANOVA with Brown-Forsythe and Welch test was done. **C)** Z-score analysis

826 showing the excluded candidate proteins and the absence of any effect on SARS-CoV-2 S
827 pseudotyped VLP entry. The dotted lines at -3 and +3 are thresholds that correspond to 3
828 times the standard deviation. The asterisk represents knockout of A549 A2T2 cells using a 2nd
829 gRNA. **D)** Z-score depicting the absence of any effect of the excluded proteins on VSV-G
830 pseudotyped VLP entry. The dotted lines at -3 and +3 are thresholds that correspond to 3
831 times the standard deviation. The asterisk represents knockout of target proteins in A549
832 A2T2 cells with a 2nd gRNA.
833
834 **Figure S6: A)** Total cell lysates were separated by SDS-PAGE and analyzed by western blot to
835 verify the knockout of target proteins in Calu3 cells. ACE2 knockouts were performed as a
836 positive control. Equal loading was verified by probing for beta-actin. **B)** Quantification of
837 target proteins as shown in (A) in Calu3 cells post knockout using lentiviral gRNAs. The
838 knockouts with 2 gRNAs have been pooled together. The black circle indicates the knockout
839 using gRNA1 and the black squares indicate the knockouts made using gRNA2. One-Way
840 ANOVA statistical test was performed to compare the Calu3 control cells with the knockouts
841 of the target proteins. **C)** Total cell lysates of A549 A2T2 and Calu3 cells were separated by
842 SDS-PAGE and analyzed by western blot to verify the endogenous levels of the six target
843 proteins. Beta-actin was used as a loading control.
844
845 **Figure S7: A)** SARS-CoV-2 pseudotyped VLP entry is indicated in relative light units to ctrl in
846 A549 cells transduced with lentiviral cDNAs of target proteins. One-way ANOVA with Brown-
847 Forsythe and Welch test was done. **B)** VSV-G pseudotyped VLP entry in A549 cells
848 overexpressed with cDNAs of target proteins is depicted in relative light units to mock, ctrl.
849 One-way ANOVA with Brown-Forsythe and Welch test was done. **C)** Z-score analysis of the

SARS-CoV-2 S pseudotyped VLP entry into A549 cells overexpressed with respective cDNAs. Dotted lines at -3 and +3 are thresholds that correspond to 3 times the standard deviation. **D)** Z-score of VSV-G pseudotyped VLP entry in A549 cells overexpressed with target proteins by lentiviral transduction. Dotted lines at -3 and +3 are thresholds that correspond to 3 times the standard deviation.

Figure S8: SARS-CoV-2 S and VSV-G pseudotyped entry into A549 A2 OE cells. A) SARS-CoV-2 pseudotyped VLP entry is indicated in relative light units to ctrl in A549 A2 cells transduced with lentiviral cDNAs of target proteins. One-way ANOVA with Brown-Forsythe and Welch test was done. **B)** VSV-G pseudotyped VLP entry in A549 A2 cells overexpressed with cDNAs of target proteins is depicted in relative light units to mock, ctrl. One-way ANOVA with Brown-Forsythe and Welch test was done. **C)** Z-score analysis of the SARS-CoV-2 S pseudotyped VLP entry into A549 A2 cells overexpressed with respective cDNAs. Dotted lines at -3 and +3 are thresholds that correspond to 3 times the standard deviation. **D)** Z-score of VSV-G pseudotyped VLP entry in A549 A2 cells overexpressed with target proteins by lentiviral transduction. Dotted lines at -3 and +3 are thresholds that correspond to 3 times the standard deviation.

Figure S9: SARS-CoV-2 S and VSV-G pseudotyped entry into Calu3 cells. A) SARS-CoV-2 pseudotyped VLP entry is indicated in relative light units to ctrl in Calu3 cells transduced with lentiviral cDNAs of target proteins. One-way ANOVA with Brown-Forsythe and Welch test was done. **B)** VSV-G pseudotyped VLP entry in Calu3 cells overexpressed with cDNAs of target proteins is depicted in relative light units to mock, ctrl. One-way ANOVA with Brown-Forsythe and Welch test was done. **C)** Z-score analysis of the SARS-CoV-2 S entry into Calu3 cells overexpressed with respective cDNAs. Dotted lines at -3 and +3 are thresholds that

875 correspond to 3 times the standard deviation. **D)** Z-score of VSV-G entry in Calu3 cells
876 overexpressed with target proteins by lentiviral transduction. Dotted lines at -3 and +3 are
877 thresholds that correspond to 3 times the standard deviation.
878
879 **Figure S10: A)** Total cell lysates were separated by SDS-PAGE and analyzed by western blot to
880 check for over expression of target proteins in A549 cells. Over expression of ACE2 in A549
881 cells was done as a positive control **B)** Total cell lysates were separated by SDS-PAGE and
882 analyzed by western blot to check for over expression of target proteins in A549 A2 cells. **C)**
883 Total cell lysates were separated by SDS-PAGE and analyzed by western blot to check for over
884 expression of target proteins in Calu3 cells.
885
886 **Figure S11: A)** Calu3 cells were treated with KYT0353 (100 µM) for 2 h and intracellular ATP
887 levels were measured at 2 h+ 24 h, 48 h, 72 h and 96 h post pretreatment. Three technical
888 repeats from one experiment are shown. DMSO was used as a solvent control. Two-way
889 ANOVA was performed as a statistical test. **B)** Calu3 cells were treated with KYT0353 (500 µM)
890 for 2 h and intracellular ATP levels were measured at 2 h+ 24 h, 48 h, 72 h and 96 h post
891 pretreatment. Three technical repeats from one experiment are shown. DMSO was used as a
892 solvent control. Two-way ANOVA was performed as a statistical test. **C)** Calu3 cells were
893 pretreated with GI254023X 100 µM for 4 h and intracellular ATP levels were measured at 4 h+
894 24 h, 48 h, 72 h and 96 h post pretreatment. Three technical repeats from one experiment are
895 shown. DMSO was used as a solvent control for GI254023X. Two-way ANOVA was performed
896 as statistical test **D)** Intracellular ATP levels were measured after 2 h+ 24 h, 48 h, 72 h and 96
897 h of Camostat mesylate at 100 µM and Ouabain treatment at 10 nM in Calu3 cells, three
898 technical repeats from one experiment are shown. H2O was used as a solvent control for

899 Camostat mesylate and Ouabain treatment. Two-way ANOVA was performed as statistical
900 test.
901
902 **Table S1:** List of proteins present in all 3 or 2 out of the 3 mass spectrometry experiments. The
903 six proteins highlighted in red were selected as target proteins for follow-up experiments.
904 These target proteins are involved in the entry mechanisms of other viruses. The name of the
905 virus along with the corresponding reference is shown in the table.
906
907 **Table S2:** IC50 concentrations according to literature for GI254023X, KYT0353, Ouabain and
908 Camostat mesylate are indicated.
909

A

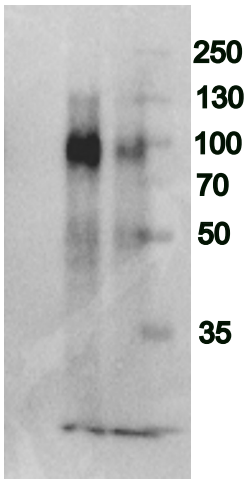

IP

B

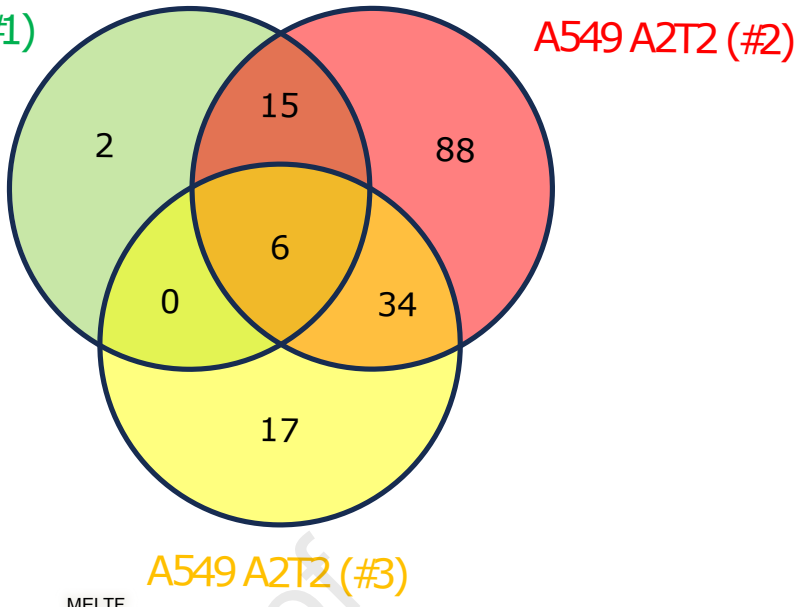

C

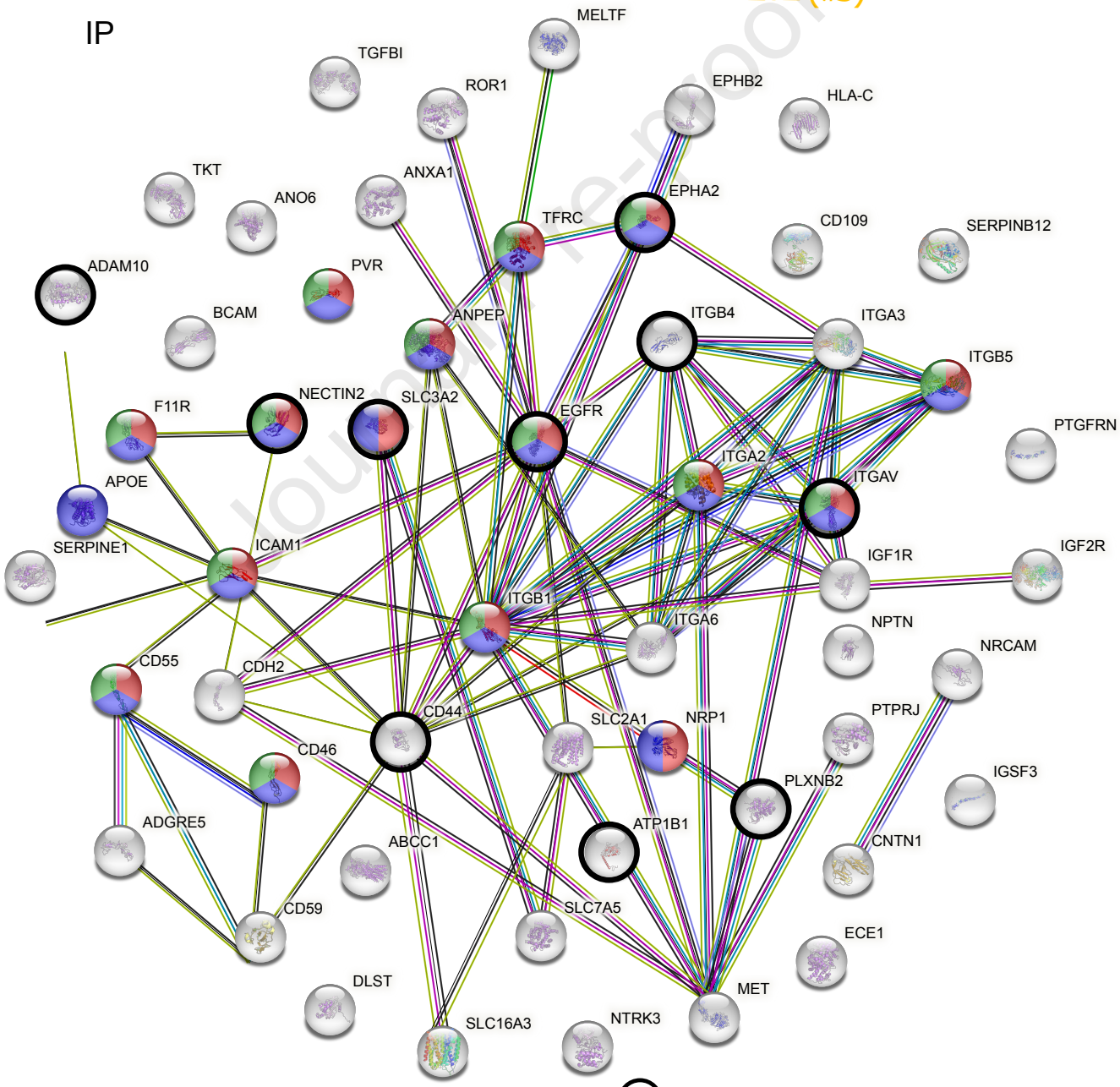

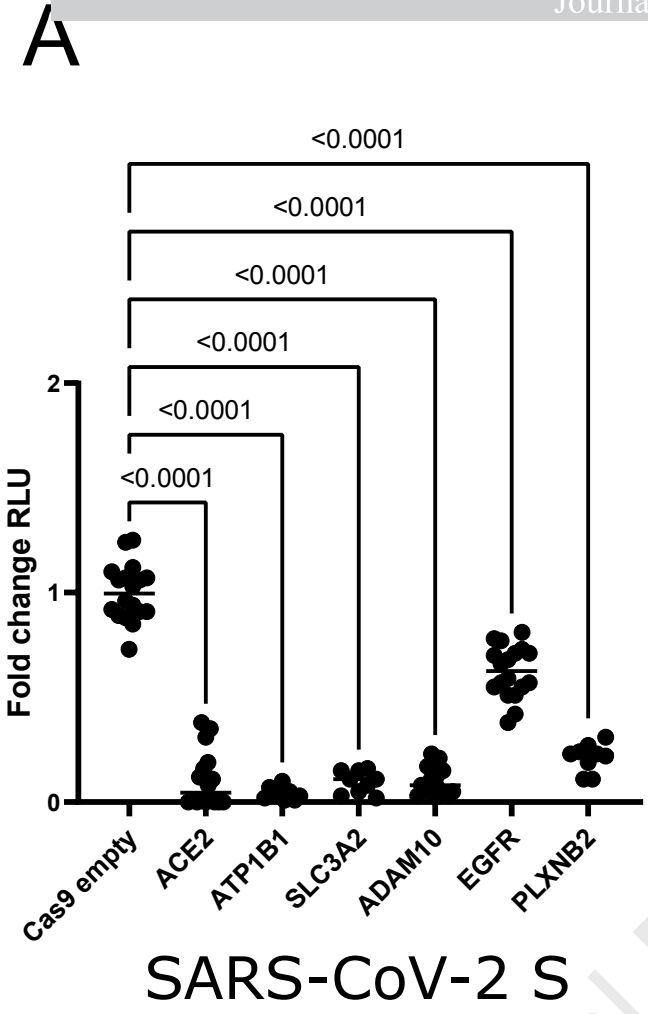

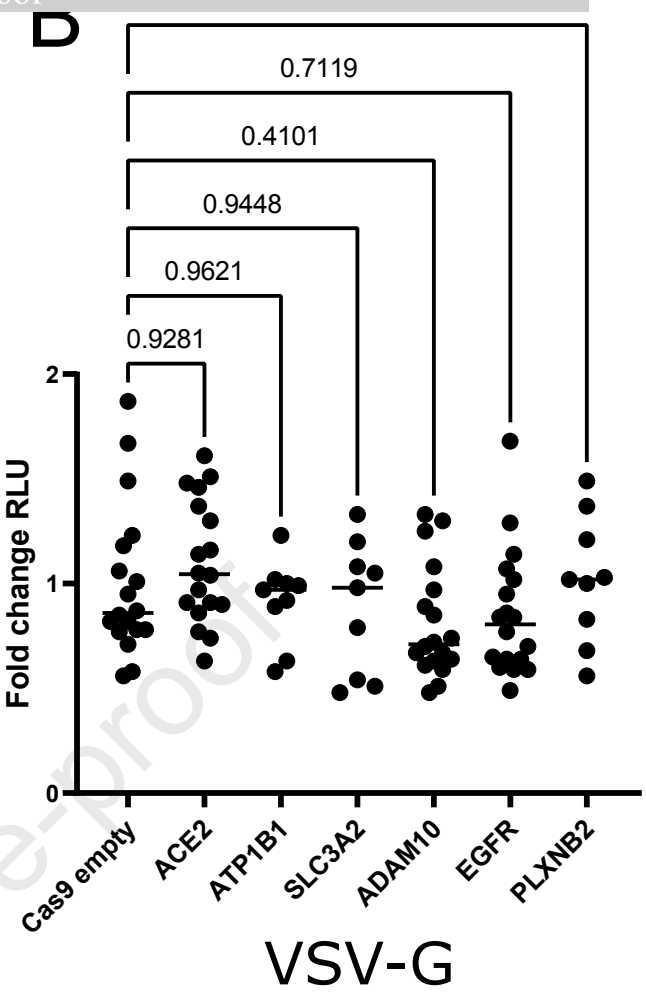

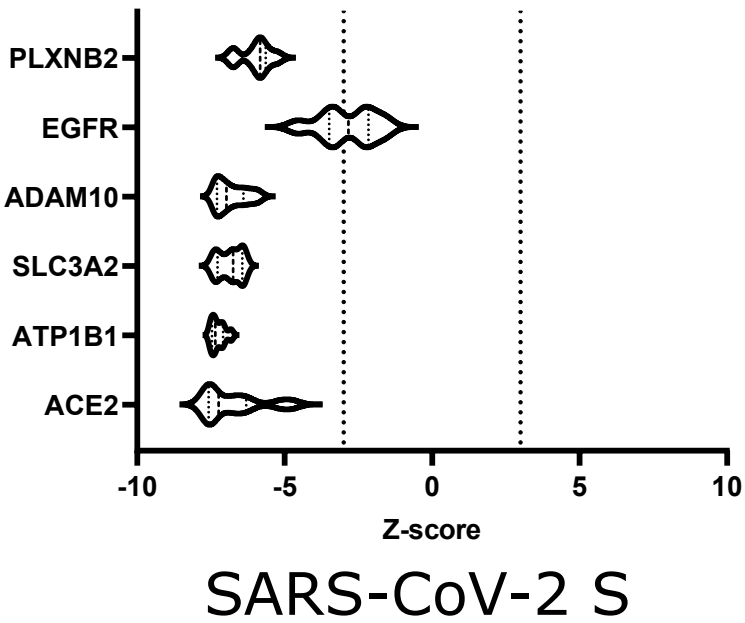

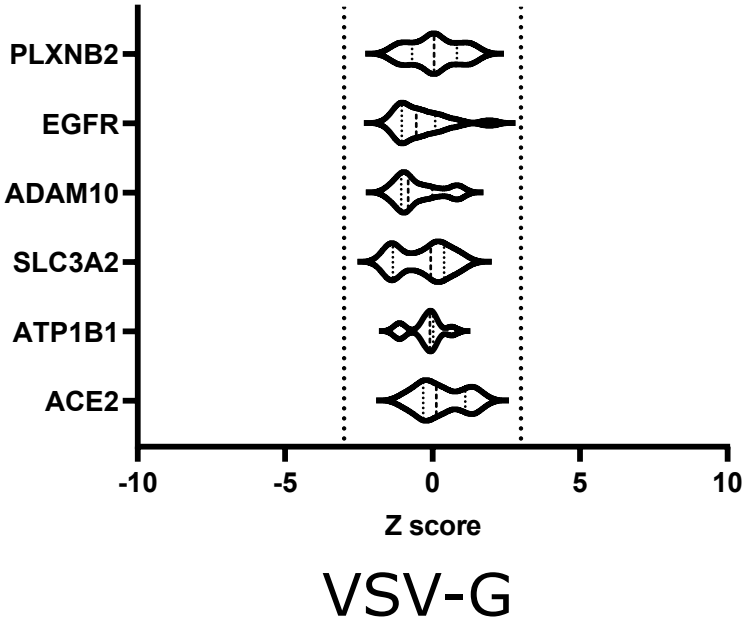

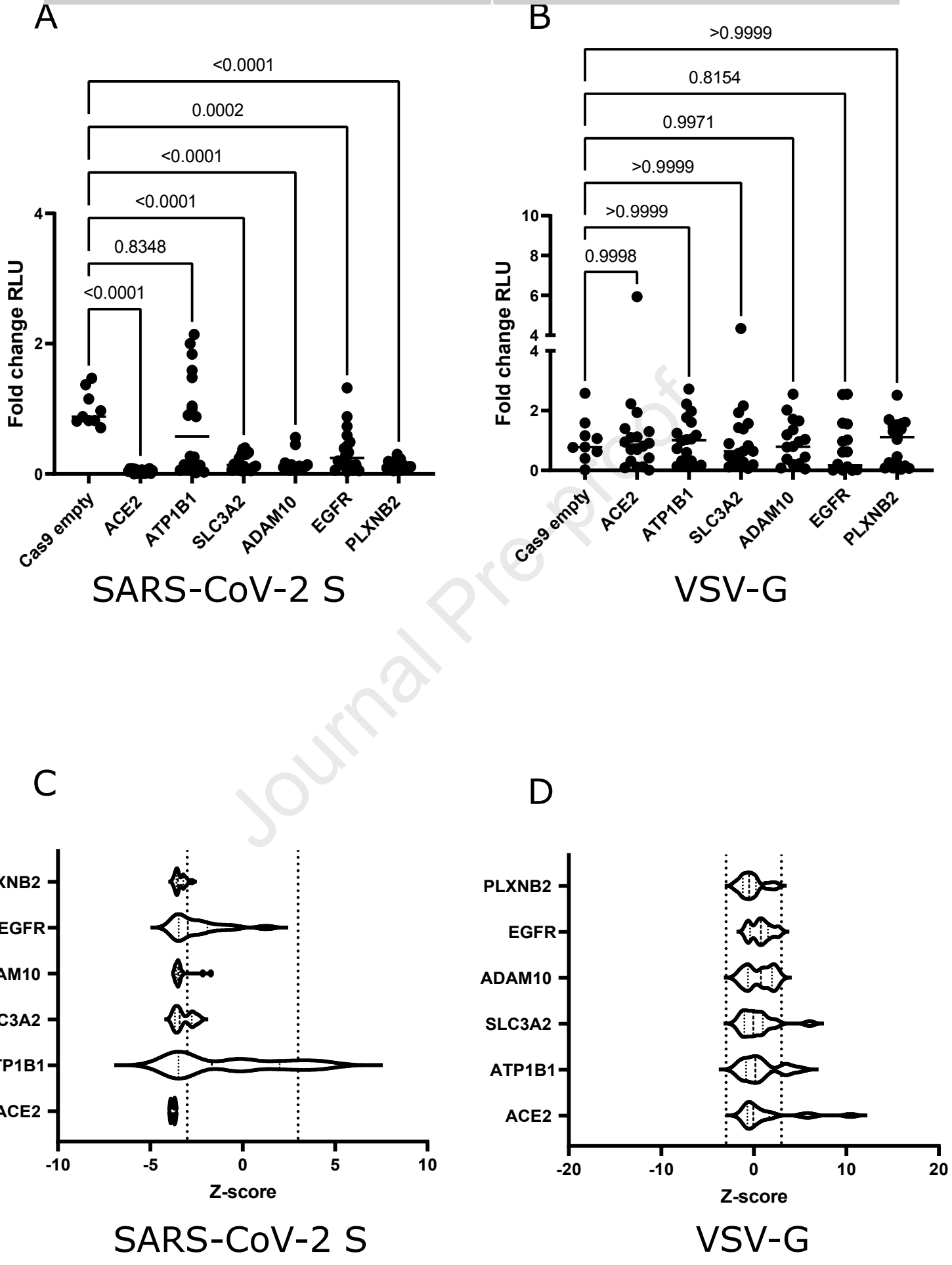

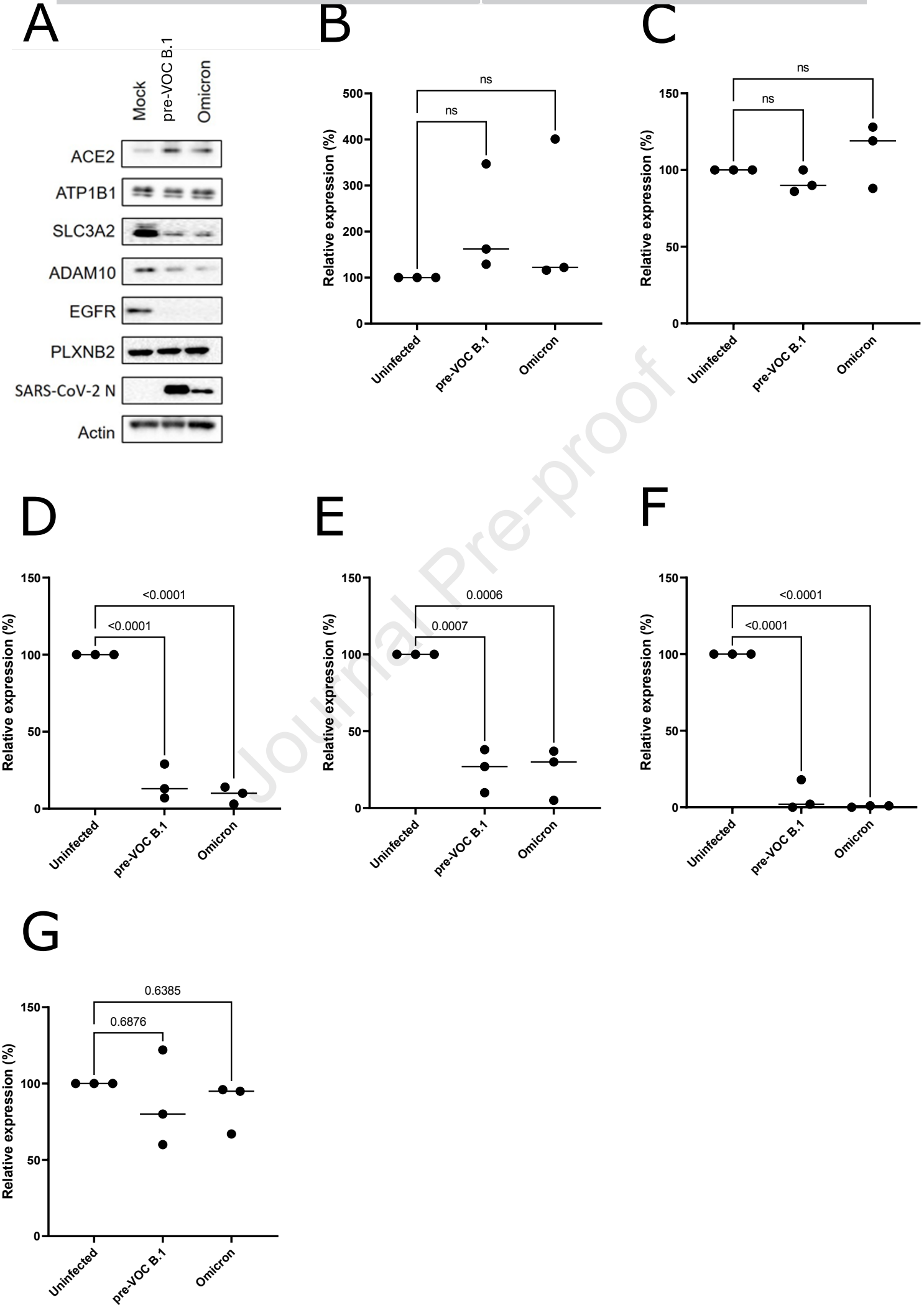

A

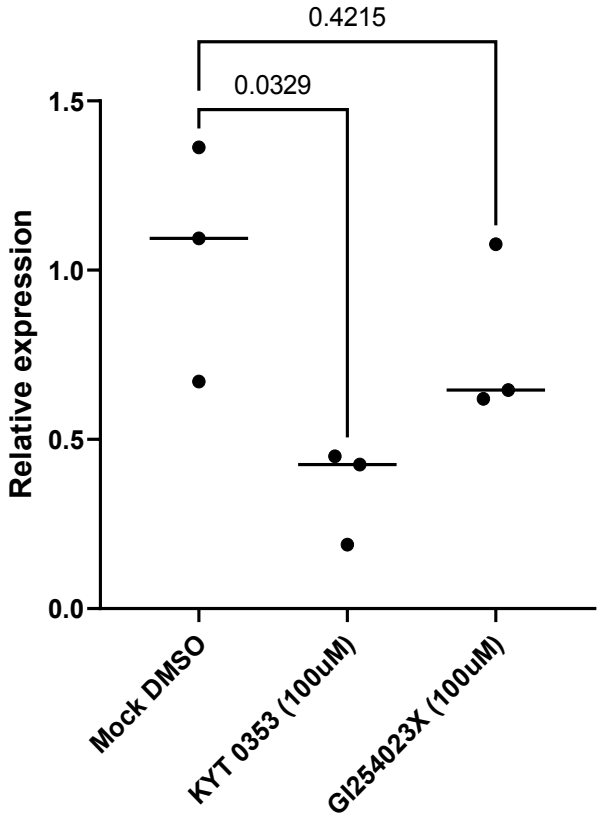

B

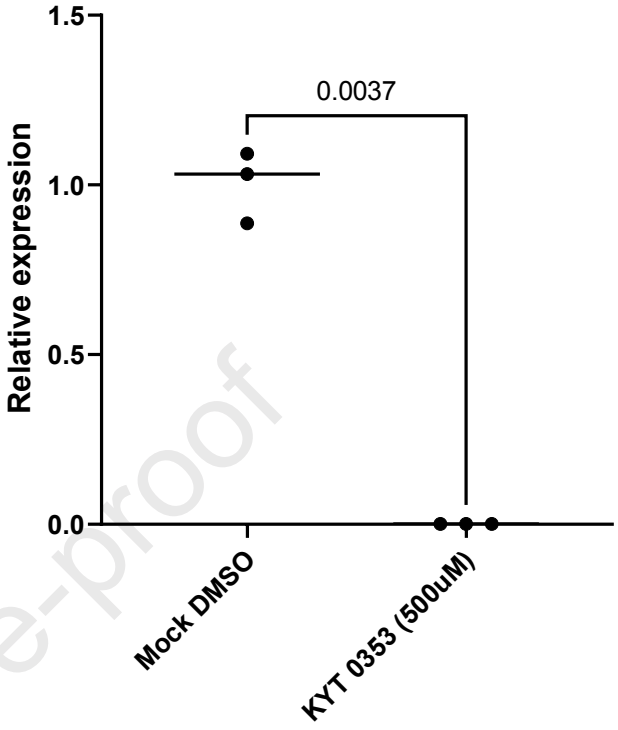

C

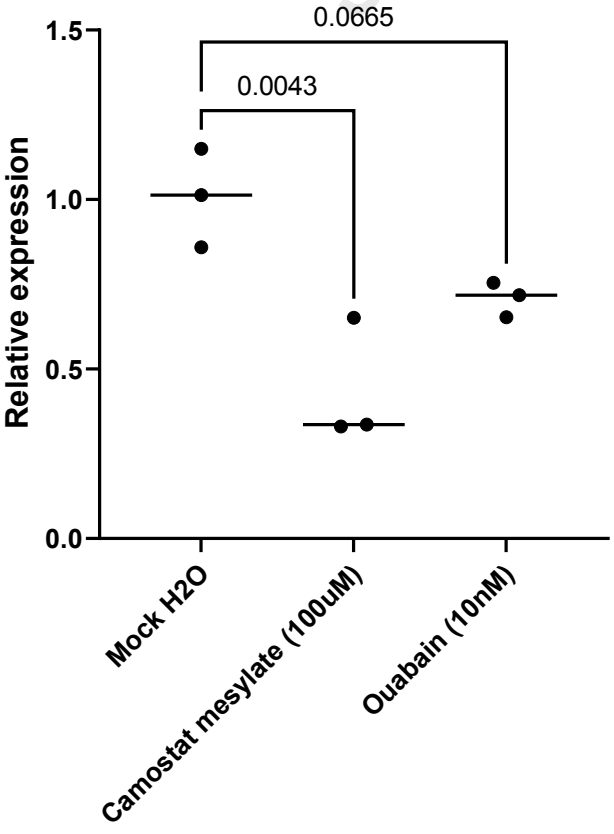

Highlights

- SLC3A2 and ADAM10 are host dependency factors for SARS-CoV-2 entry
- SLC3A2 can be targeted with available inhibitors to diminish SARS-CoV-2 entry
- Cell surface proximity ligation identifies antiviral targets

Declaration of interests

☒ The authors declare that they have no known competing financial interests or personal relationships that could have appeared to influence the work reported in this paper.

☐The authors declare the following financial interests/personal relationships which may be considered as potential competing interests: